# First-Principles, All-Electron Calculation of Electronic Stopping for Crystals in the Dielectric Formulation

Richard J. Mathar, S. B. Trickey, and John R. Sabin
*Quantum Theory Project, Department of Physics, Univ. of Florida, Gainesville, FL 32611-8435*
(17th Werner Brandt Workshop, 8-9 May 1997; Corrected version 20 July 1997)

Charged projectile energy loss to an electron population in finite systems (e.g. molecules) is a probe of the target's generalized oscillator strength spectrum. First principles calculation of the GOS spectrum over a large range of momenta for real molecules is an extremely challenging task which we considered at the 15th WBW.[1]

For ordered extended systems (crystals, ultra-thin films), the corresponding quantity is the inverse of the wave-vector and frequency- dependent dielectric matrix $\epsilon_{\mathbf{GG}'}(\mathbf{k},\omega)$, in particular, the zero-zero element of its inverse, $K_{\mathbf{GG}'}$. The dielectric matrix is determined by the irreducible polarizability $\Pi$, a Brillouin Zone integral and energy band sum over the squared magnitude of matrix elements akin to those in the GOS, weighted by energy denominators and Fermi occupation factors.[2–4]

With the goal of calculating $\Pi$ and $dE/dx$ from first principles, all-electron Kohn-Sham states associated with calculated equilibrium lattice parameters, the computation of $\Pi$ over the minimally useful range of energy transfers (100 eV) and momentum transfers (five or more reciprocal lattice vectors) is a demanding task, even in the random phase approximation. Within the RPA, we report on algorithmic choices, code design criteria, implementation, testing, and preliminary physical results of such a calculation.

## I. DIELECTRIC RESPONSE - BULK CRYSTALS

### A. Electronic Stopping

The objective of the research reported here is provision of a quantitative, predictive, materials-specific, first-principles description of the process of energy deposition by a bare ion in a material target. The target itself is to be characterized computationally in a chemically specific and predictive way. For simplicity we consider only protons, thus avoid having to deal with the additional complication of dynamic charge states of the projectile. This paper has the status of a progress report.

The linear energy loss (stopping power) of a massive, charged particle to a target generally is related to the velocity-dependent stopping cross section by

$$-\frac{dE}{dx} = \mathcal{N} S(\mathbf{v})$$

where $\mathcal{N}$ is the macroscopic target matter density, and $\mathbf{v}$ is the projectile velocity in the lab frame. $Z_1$ will denote the projectile charge number, and $m$ the electron mass. In SI units the energy loss per unit path length is

$$\frac{dE}{dx} = \frac{(Z_1 e)^2}{4\pi^3 \epsilon_0 v} \int d^3q \frac{\mathbf{v}\cdot\mathbf{q}}{q^2} \int_0^\infty d\omega \delta(\omega - \mathbf{q}\cdot\mathbf{v}) \Im K_{\mathbf{00}}(\mathbf{q},\omega). \tag{1}$$

Here $\mathbf{G}$ is a reciprocal lattice vector, $K_{\mathbf{00}}$ is the $\mathbf{G} = \mathbf{G}' = \mathbf{0}$ ("head") component of the inverse dielectric matrix defined by

$$\sum_{\mathbf{G}'} \epsilon_{\mathbf{G},\mathbf{G}'}(\mathbf{q},\omega) K_{\mathbf{G}',\mathbf{G}''}(\mathbf{q},\omega) = \delta_{\mathbf{GG}''}$$

with respect to $\epsilon_{\mathbf{G}',\mathbf{G}''}(\mathbf{k},\omega)$, the frequency and wave-vector dependent microscopic dielectric matrix. [Eq. (1) ignores contributions $\propto \exp(i\mathbf{G}\cdot\mathbf{v}t)$, which are in general rapidly oscillatory or require hyperchanneling ($\mathbf{G} \perp \mathbf{v}$).]

For the case of longitudinal response alone, the dielectric displacement $D$ resulting from the *total* electrical field $E$ is described by $\epsilon_{\mathbf{G},\mathbf{G}'}$ as

$$D(\mathbf{q}+\mathbf{G},\omega) = \epsilon_0 \sum_{\mathbf{G}'} \epsilon_{\mathbf{G},\mathbf{G}'}(\mathbf{q},\omega) E(\mathbf{q}+\mathbf{G}',\omega)$$

with $\mathbf{q}$ the wave vector of the *external* field.

The dielectric matrix itself is

$$\epsilon_{\mathbf{G},\mathbf{G}'}(\mathbf{q},\omega) = \delta_{\mathbf{GG}'} - \frac{e^2}{\epsilon_0 |\mathbf{q}+\mathbf{G}|^2} \Pi(\mathbf{q}+\mathbf{G},\mathbf{q}+\mathbf{G}',\omega),$$

and the irreducible polarizability $\Pi$ is given in detail below.

### B. Predictions with Material and Chemical Specificity

Though calculations of $\epsilon_{\mathbf{G},\mathbf{G}'}(\mathbf{q},\omega)$ have been a recurring topic since the beginnings of computational solid state physics roughly 40 years ago, there remain significant unsolved problems. Early calculations frequently reduced the problem to a joint density of states via the convenient but crude approximation of constant matrix elements for the irreducible polarizability; see for example the study in Ref. 5. Whatever the level of approximation, early calculations tended to focus on properties such as the optical conductivity or the static screening, hence omit either the frequency or wave-vector dependence; see Refs. 6, 7 for examples. Another body of work, related largely to energy gaps in semiconductors, has used model dielectric functions to provide the screened Coulomb potential in the $GW$ approximation; see Ref. 8 for citations of the original work.

There is a vast literature of dielectric treatments of energy deposition including of course by Werner Brandt[9] himself, Lindhard and Winther[10], Kitagawa[11], Kaneko[12] and many others. The majority of papers have used one or another variant on the theme of $\epsilon$ from the homogeneous electron gas; in addition to the examples just cited see the local density approximation scheme of the San Sebastian group[13] for another.

Energy deposition calculations intended for use in materials and surface physics and chemistry must account for characteristics of the target system in a materials-specific, chemically specific, predictive way. The obligation of computational theory is to predict the lattice structure of the target (either at equilibrium or under specified constraints; we restrict discussion to targets ordered in at least two Cartesian dimensions) on the basis of microscopic treatment of the electron population, then calculate the desired energy deposition cross section [here, $S(\mathbf{v})$] from that microscopic knowledge. The potential impact of system structure upon electronic response is illustrated by crystalline Al. Experimentally a decrease of only 8% in lattice constant (achieved at $P = 310$ kbar) causes a drastic qualitative change in the optical conductivity:[14] one peak at about 1.5 eV splits into two (at 1.5 and 2.5 eV).

### C. Aspects of Density Functional Theory

Density functional theory (DFT) is the pre-eminent formal basis for calculation of material properties and electronic structure today. DFT is based on the theorems of Hohenberg, Kohn, and Sham (HKS) which prove the existence, uniqueness, and variational stability of the ground state total energy of a many-electron system as a functional of its electron density (or spin densities) alone. HKS also showed how to carry out the variation via what is now called the Kohn-Sham (KS) procedure.

Because HKS gave existence theorems, they provided no explicit form for the energy functional. To this date the great majority of DFT calculations is based on the local spin density approximation (LSDA). It provides an approximate functional which gives both the spin densities and the total energy in terms of the spin orbitals of a reference non-interacting many-electron system. The two systems are constrained to be equivalent in that both have the same ground state densities. The variation principle then gives the KS equations (in a slightly abridged notation regarding spin dependencies)

$$\left\{-\frac{\hbar^2}{2m}\nabla^2 + V_\sigma[\rho(\mathbf{r})]\right\}\varphi_{\nu,\mathbf{k},\sigma}(\mathbf{r}) = \varepsilon_{\nu,\mathbf{k},\sigma}\varphi_{\nu,\mathbf{k},\sigma}(\mathbf{r}),$$

where the spin number density $\rho_\sigma$ is given by

$$\rho_\sigma(\mathbf{r}) = \sum_{\nu,\mathbf{k}} f_{\nu,\mathbf{k},\sigma}|\varphi_{\nu,\mathbf{k},\sigma}(\mathbf{r})|^2.$$

The local potentials $V_\sigma[\rho(\mathbf{r})]$ contain electron-electron Coulomb repulsion, exchange-correlation (XC), and nuclear-electron attraction terms. The XC potentials are the ones approximated in LSDA.

The task is to solve the KS equations and determine the lowest energy structure and lattice parameters, then use the KS orbitals and eigenvalue differences to construct $\Pi$. Such use of the KS orbitals and eigenvalues is not rigorous, but has proven to be quite reasonable in both $GW$ calculations (recall above) and in other studies which tested the issue.[15]

The code used to solve the KS equations and find the energy minimum configuration for both 2D (ultra-thin films, slabs, both without supercells) and 3D infinitely periodic systems (solids) is the computational package GTOFF.[16,17] It performs all-electron, full-potential, linear combination of Gaussian Type Orbitals (GTO's) calculations via so-called Fitting Function algorithms. Those algorithms handle the highly non-linear dependence of the KS potentials upon the spin densities (hence, upon the KS orbitals) via intermediate linear expansion in an auxiliary Gaussian basis set and accelerate the Coulomb integrals by an auxiliary expansion as well. There are no pseudopotentials, muffin-tin potentials, nor frozen cores. In the case of an ultra-thin film (UTF), no inversion symmetry is required through the plane of the UTF, nor are supercells required. Although we have studied proton stopping in UTF's, here we consider *only* solids.

### D. RPA and Matrix Elements - Strategy

In the Random Phase Approximation, $\Pi$ is[2]

$$\Pi(\mathbf{q}+\mathbf{G},\mathbf{q}+\mathbf{G}',\omega) = \sum_{\nu\nu'}\int_{\mathrm{BZ}}\frac{d^3k}{(2\pi)^3}\frac{m^*_{\mathbf{G}}m_{\mathbf{G}'}(f_{\nu\mathbf{k}} - f_{\nu'\mathbf{k}+\mathbf{q}})}{\hbar\omega + i\eta + \varepsilon_{\nu\mathbf{k}} - \varepsilon_{\nu'\mathbf{k}+\mathbf{q}}} \qquad (2)$$

where $\nu, \nu'$ are band indices, $f_{\nu\mathbf{k}}$ are Fermi factors (2 or 0) for wave vector $\mathbf{k}$, and $\varepsilon_{\nu,\mathbf{k}}$ are the KS band energies. The integral is over the first Brillouin zone (BZ), but can be evaluated equivalently (and more conveniently) over a primitive unit cell of the reciprocal lattice.

The matrix elements in (2) are given by

$$m_{\mathbf{G}} \equiv \langle\nu'\mathbf{k}+\mathbf{q}|e^{i(\mathbf{G}+\mathbf{q})\mathbf{r}}|\nu\mathbf{k}\rangle.$$

Identification of the lattice-periodic part $u$ of the Bloch functions

$$\psi_{\nu,\mathbf{k}}(\mathbf{r}) = e^{i\mathbf{k}\mathbf{r}}u_{\nu\mathbf{k}}(\mathbf{r}),$$

and their plane wave expansion coefficients,

$$u_{\nu\mathbf{k},\mathbf{G}} \equiv \int_{\mathrm{UC}} e^{-i\mathbf{G}\mathbf{r}} u_{\nu\mathbf{k}}(\mathbf{r}) d^3 r,$$

leads to a formula of the correlation type for the matrix elements,

$$m_{\mathbf{G}} = \frac{1}{V_{\mathrm{UC}}} \sum_{\mathbf{K}} u^*_{\nu',\mathbf{k}+\mathbf{q},\mathbf{K}}\, u_{\nu,\mathbf{k},\mathbf{K}-\mathbf{G}},$$

with $V_{\mathrm{UC}}$ the volume of the unit cell.

Note that the computational strategy adopted here is to make a transformation from the GTO basis to a plane wave basis, hence gain speed from the simplicity of the formulation at the cost of storage. A secondary virtue is that representations from plane-wave based methods could be coupled relatively straightforwardly to our dielectric function code package.

### E. Exploitable Symmetries

The symmetry of the one-particle potential in the KS equation with respect to a point group operation $O$

$$V(\mathbf{r}) = V(O\mathbf{r})$$

establishes a corresponding symmetry of the Bloch functions and therefore of the irreducible polarizability and the dielectric matrix[18]

$$\epsilon_{\mathbf{G},\mathbf{G}'}(\mathbf{q},\omega) = \epsilon_{O\mathbf{G},O\mathbf{G}'}(O\mathbf{q},\omega).$$

For large $|\mathbf{q}|$, the following shift property enables coverage in terms of elements at smaller vectors, to wit

$$\epsilon_{\mathbf{G},\mathbf{G}'}(\mathbf{q},\omega) = \epsilon_{\mathbf{G}+\mathbf{G}'',\mathbf{G}'+\mathbf{G}''}(\mathbf{q}-\mathbf{G}'',\omega) \qquad \forall \mathbf{G}''.$$

These symmetry properties are also valid for the product $|\mathbf{q}+\mathbf{G}|^2 \epsilon_{\mathbf{G},\mathbf{G}'}(\mathbf{q},\omega)$, which exhibits less singular behavior in the long wavelength limit than the dielectric matrix itself. The inverse dielectric matrix $K$ has corresponding features.

The dielectric matrix is Hermitian, if the product of matrix elements in (2) is real, a property which can be attained, for example, by moving the origin of the real-space coordinate system to an inversion center of $V(\mathbf{r})$ (if such a center exists). It is also Hermitian in the static limit.[19]

Invariances with respect to the little group of $\mathbf{q}$ have not been exploited. The accelerations which would result would be restricted to points of high symmetry, therefore of dwindling value with increasing denseness of reciprocal space meshes.

A shift of the origin of the unit cell (UC) by an amount $\mathbf{b}$ changes the phase of the Fourier Transform (FT) of the Bloch functions, the matrix elements, and the non-diagonal elements of the irreducible polarizability and dielectric matrix

$$\begin{aligned} u_{\nu\mathbf{k}}(\mathbf{r}) &\Rightarrow u_{\nu\mathbf{k}}(\mathbf{r}+\mathbf{b}), \\ u_{\nu\mathbf{k},\mathbf{G}} &\Rightarrow e^{i\mathbf{G}\mathbf{b}} u_{\nu\mathbf{k},\mathbf{G}}, \\ m_{\mathbf{G}} &\Rightarrow e^{-i\mathbf{G}\mathbf{b}} m_{\mathbf{G}}, \\ \epsilon_{\mathbf{G},\mathbf{G}'}(\mathbf{q},\omega) &\Rightarrow e^{i(\mathbf{G}-\mathbf{G}')\mathbf{b}} \epsilon_{\mathbf{G},\mathbf{G}'}(\mathbf{q},\omega). \end{aligned}$$

The "macroscopic" energy loss function $\Im K_{\mathbf{00}}(\mathbf{q},\omega)$ is unaffected, but channeling calculations[20] specify a particular "classical" ion path through these phase factors in the elements $K_{\mathbf{G}\neq\mathbf{G}'}$.

### F. Implementation

#### 1. DFT Input

As discussed, we take the Bloch functions $|\nu\mathbf{k}\rangle$ to be the KS orbital solutions from GTOFF. Those self-consistent solutions are expressed as a superposition of Hermite GTO's

$$\begin{aligned} \psi_{\nu,\mathbf{k}}(\mathbf{r}) &\equiv \varphi_{\nu,\mathbf{k}}(\mathbf{r}) \\ &= \sum_{\mathbf{R}} e^{i\mathbf{k}\mathbf{R}} \sum_{b} c_{\nu\mathbf{k}b} N_{n\alpha}\, g(n,\alpha,\mathbf{r}-\mathbf{R}-\mathbf{r}_b) \end{aligned} \qquad (3)$$

with

- $\mathbf{R}$... real-space lattice vectors
- $N_{n\alpha}$... normalization constants
- $c_{\nu\mathbf{k}b}$... expansion coefficients for basis function $b$, including intra/inter-site contraction coefficients
- $\mathbf{r}_b$... center of the GTO relative to the origin of the UC
- $g(n,\alpha,\mathbf{r}-\mathbf{A})$... primitive GTO centered at site $\mathbf{A}$ with exponent $\alpha$
- $n$... triple index for the type ($s$, $p_{x,y,z}$, $d_{zz}$...) of the primitive GTO

In addition to the usual approximations of a finite basis set expansion, there are two approximations made by adopting (3). Explicitly that choice presumes that the KS Bloch states are reasonable approximations to the proper quasi-particle Bloch states (see above). Implicitly there is the use of the associated KS eigenvalues in the energy denominator of (2). At least the procedure is well-defined and can be improved upon in various ways, ranging upward in sophistication from simple scissors operators.

### 2. Matrix Elements

The transformation from GTO's to plane waves $u_{\nu,\mathbf{k},\mathbf{G}}$ proceeds efficiently via the FT of primitive Hermite GTOs, expressible in closed form as

$$\int d^3r\, e^{i\mathbf{qr}} g(n,\alpha,\mathbf{r}) = \left(\frac{\pi}{\alpha}\right)^{3/2} e^{-q^2/(4\alpha)} \prod_{l=x,y,z} (iq_l)^{n_l},$$

which is slightly simpler than for Cartesian GTOs.[21] The equivalence of the plane wave representation is controlled by monitoring the accumulated norm for each $|\nu,\mathbf{k}\rangle$ relative to the exact values, $\sum_{\mathbf{G}} |u_{\nu,\mathbf{k},\mathbf{G}}|^2 = V_{\mathrm{UC}}$ for normalized $\int_{\mathrm{UC}} |\varphi_{\nu,\mathbf{k}}(\mathbf{r})|^2 d^3r = 1$.

### 3. Linear Analytical Tetrahedron Method

Integration (summation) over BZ's via the Linear Analytical Tetrahedron Method, the higher dimensional analogue of the trapezoidal rule, is well-known in solid and surface electronic structure calculations.[6,22] We subdivide the integration region of the integral (2) into parallelopipeds, then subdivide each of those into six tetrahedra. Further subdivision of a given tetrahedron into smaller tetrahedra is done if one or both Fermi functions run through it, as may happen in metals. Next comes linearization of the product of the matrix elements in the numerator and of the energy denominator inside each tetrahedron for each $\omega$. Finally the resulting approximated integral is evaluated analytically after an affine coordinate transformation into the unit tetrahedron.

The contribution generated by the term $i\eta$ in the denominator of (2) ("real transitions") is, in the coordinate system of the unit tetrahedron, proportional to

$$\begin{aligned}&\int_0^1 dr_1 \int_0^{1-r_1} dr_2 \int_0^{1-r_1-r_2} dr_3 \\ &\times(C_0 + C_1r_1 + C_2r_2 + C_3r_3)\delta(b_0 + b_1r_1 + b_2r_2 + b_3r_3) \\ &= \frac{1}{b_3}\int_0^1 dr_1 \int_0^{r_m} dr_2 (T_0 + T_1r_1 + T_2r_2);\end{aligned}$$

with

$$\begin{aligned}&T_i \equiv C_i - C_3\frac{b_i}{b_3} \quad (i = 0,1,2), \\ &r_m \equiv \max[1-r_1, -\frac{b_0}{b_2} - \frac{b_1}{b_2}r_1, \frac{b_3+b_0}{b_3-b_2} - \frac{b_3-b_1}{b_3-b_2}r_1].\end{aligned}$$

Here $C_0$ is the matrix element product $m^*_{\mathbf{G}} m_{\mathbf{G}'}$ evaluated at the vertex labeled zero and similarly $b_0$ is the energy denominator $\hbar\omega + \varepsilon_{\nu\mathbf{k}} - \varepsilon_{\nu'\mathbf{k+q}}$ evaluated at that vertex. The remaining $C_i$ are the difference between the matrix element product at the i-th vertex and $C_0$ and similarly for the $b_i$. The resulting integrals of linear functions over trapezoids have simple analytical solutions. The full integral (2) is then extracted efficiently from this intermediate result by a Kramers-Kronig (Hilbert) transformation.[23] To avoid numerical difficulties stemming from direct evaluation of the principle value in the K-K transform, we exploit the fact that it is expressible as a convolution with $\frac{1}{\omega}$, hence can be implemented as a Fourier Transform into the time domain, multiplication with $2\Theta(t)$, then an inverse FT back into the frequency domain. With careful use of a standard FFT, the results are numerically reliably.

## G. Other Matters of Technique

Currently, the product $|\mathbf{q}+\mathbf{G}|^2\epsilon_{\mathbf{G},\mathbf{G}'}(\mathbf{q},\omega)$ is calculated and, in compensation, the term $q^2$ in the denominator of (1) is dropped (cancellation of divergences). The dielectric function is tabulated for $\mathbf{q}$ commensurate with the mesh of wave vectors used in the underlying GTOFF calculation but covering higher BZs as well as the first. $\Im K_{\mathbf{G},\mathbf{G}'}$ is linearized inside each $\mathbf{q}$-space tetrahedron. Multiplied by the linear factor $\mathbf{q}\cdot\mathbf{v}$, the integrals (1) over tetrahedra are done analytically, then summed up.

Evaluation of Eq. (1) involves a region of integration which covers the half-infinite "triangle"

$$0 \le \omega \le \mathbf{q}\cdot\mathbf{v}$$

of combined energy and momentum transfers.

# II. HEXAGONAL BULK LITHIUM

## A. Structure

The hexagonal close packed form of solid lithium is most probably the stable form at zero temperature, if more complicated close-packed structures are left aside.[24] A survey of the calculated structure-energy relationships for fcc, hcp, and bcc Li is in Boettger *et al.*[25] The question whether hcp or bcc (the room temperature phase) is predicted to be more stable by modern DFT calculations was resolved by Nobel *et al.*[26] in favor of hcp. However the KS band structure for equilibrium hcp Li apparently has not been published, hence see Figs. 1–2. These (and the associated KS orbitals) are the inputs to the results which follow.

## B. Computed Electronic Energy Loss by Protons

The following results are preliminary. The computed dielectric functions satisfy the essential sum rules[27] to within 9% for the two valence electrons in the unit cell, provided the frequency integration is restricted to lie below the K-shell excitation, roughly 45 eV. For upper limits through 60 eV, the all-electron sum rule value is still rising. How close the the well-known problem of finite basis sets discussed by two of us at WBW-15[1] lies is not evident.

The influence of the local field effects, i.e., of the "wing" (first row and first column) and "body" (co-factor of the head element) matrix elements remains small for lithium. Figures 3–4 show for comparison $\Im\epsilon_{\mathbf{G},\mathbf{G}'}(\mathbf{q},\omega)$ of the "head" element $\mathbf{G} = \mathbf{G}' = \mathbf{0}$ and of the "body" element $\mathbf{G} = \mathbf{G}' = (0001)$. Values above 45 eV include excitations from the Li $K$-shell (the lowest band in the band structure). "Local field effects" are not included in Fig. 5, in so far as $\Im 1/\epsilon_{\mathbf{0},\mathbf{0}}$ instead of $\Im K_{\mathbf{0},\mathbf{0}}$ is shown.

The energy loss cross-sections $S$ shown in the two Figures 6 –7 are based on a coarser GTOFF input of $6\times6\times4$ points in the BZ (21 points in the IBZ), using only the $\mathbf{G} = \mathbf{G}' = \mathbf{0}$ element of the dielectric matrix. Values outside the meshes were replaced by the vacuum response, $\epsilon_{\mathbf{G},\mathbf{G}'}(\mathbf{q},\omega) = \delta_{\mathbf{G},\mathbf{G}'}$. The oscillatory behavior of $S(\mathbf{v})$ for $v \gtrapprox v_0$ is an unmistakable indication of this limitation.

## ACKNOWLEDGMENT

Support by grant DAA-H04-95-1-0326 from the U.S. Army Research Office is gratefully acknowledged.

---

[1] S.B. Trickey, J.R. Sabin, J.A. Nobel, and J. Oddershede, 15th Werner Brandt Workshop, 10–11 Mar. 1994; E.H. Mortensen, J. Oddershede, and J.R. Sabin, Nucl. Instr. Meth. B **69**, 24 (1992).

[2] S.L. Adler, Phys. Rev. **126**, 413 (1962); N. Wiser, Phys. Rev. **129**, 62 (1963); D.S. Falk, Phys. Rev. **118**, 105 (1960); O.V. Dolgov and E.G. Maksimov in *The dielectric function of condensed systems*, vol. 14 of *Modern Problems in condensed matter sciences*, V.M. Agranovich and A.A. Maradudin eds. (North-Holland, 1989).

[3] J. Lindhard and M. Scharff, K. Dan. Vidensk. Selsk. Mat.-Fys. Medd. **27**, No. 15 (1953).

[4] U. Fano, Ann. Rev. Nucl. Sci. **13**, 1 (1963) *Stopping powers and ranges in all elements*, (Pergamon, New York, 1977)

[5] A.R. Lubinsky, D.E. Ellis, and G.S. Painter, Phys. Rev. B **6**, 3950 (1972).

[6] S.P. Singhal, Phys. Rev. B **12**, 564 (1975).

[7] W.Y. Ching and J. Callaway, Phys. Rev. B **9**, 5115 (1974).

[8] M.S. Hybertsen and S.G. Louie in *Density Functional Theory of Many-Fermion Systems*, S.B. Trickey special ed., Adv. Quantum Chem. **21**, 155 (1990).

[9] W. Brandt, Phys. Rev. **111**, 1042 (1958).

[10] J. Lindhard and A. Winther, K. Dan. Vidensk. Selsk. Mat.-Fys. Medd. **34**, No. 4 (1964).

[11] M. Kitagawa, Vacuum **39**, 335 (1989).

[12] T. Kaneko, phys. stat. sol. (b) **156**, 49 (1989); Atom. Data Nucl. Data Tabl. **53**, 271 (1993).

[13] P.M. Echenique and M.E. Uranga in *Interaction of Charged Particles with Solids and Surfaces*, A. Gras Martí, H.M. Urbassek, N. Arista, and F. Flores, eds. (Plenum Press, NY, 1991).

[14] H. Tups and K. Syassen, J. Phys. F: Met. Phys. **14**, 2753 (1984).

[15] P. Duffy, D.P. Chong, M.E. Casida, and D.R. Salahub, Phys. Rev. A **50**, 4707 (1994).

[16] J.C. Boettger, Int. J. Quantum Chem. S-**29**, 197 (1995); J.C. Boettger and S.B. Trickey, Phys. Rev. B **53**, 3007 (1996).

[17] J.W. Mintmire, J.R. Sabin, and S.B. Trickey, Phys. Rev. B **26**, 1743 (1982); U. Birkenheuer, J.C. Boettger, and N. Rösch, J. Chem. Phys. **100**, 6826 (1994).

[18] M.S. Hybertsen and S.G. Louie, Phys. Rev. B **35**, 5585 (1987).

[19] N. Hamada, M. Hwang, and A.J. Freeman, Phys. Rev. B **41**, 3620 (1990); R. Resta and A. Baldereschi, Phys. Rev. B **23**, 6615 (1981).

[20] F. Bonsignori and A. Desalvo, J. Phys. Chem. Sol. **31**, 2191 (1979); A.F. Burenkov, F.F. Komarov, and M.A. Kumakhov, phys. stat. sol. (b) **99**, 417 (1980); T.M.H. Tielens, G.E.W. Bauer, and T.H. Stoof, Phys. Rev. B **49**, 5741 (1994); O.H. Crawford and C.W. Nestor, Jr., Phys. Rev. A **28**, 1260 (1983); L.R. Logan, C.S. Murthy, and G.R. Srinivasan, Phys. Rev. A **46**, 5754 (1992).

[21] P. Kaijser and V.H. Smith Jr, Adv. Quant. Chem. **10**, 37 (1977).

[22] J.P.A Charlesworth and W. Yeung, Comp. Phys. Comm. **88**, 186 (1995); Phys. Rev. B **53**, 2606 (1996); J. Rath and A.J. Freeman, Phys. Rev. B **11**, 2109 (1975); P.-A. Lindgård, Solid State Comm. **16**, 481 (1975).

[23] D.L. Johnson, Phys. Rev. B **9**, 4475 (1974).

[24] A.D. Zdetsis, Phys. Rev. B **34**, 7666 (1986).

[25] J.C. Boettger, S.B. Trickey, and J.A. Nobel, Phys. Rev. B **45**, 7503 (1992).

[26] J.A. Nobel, S.B. Trickey, P. Blaha, and K. Schwarz, Phys. Rev. B **45**, 5012 (1992).

[27] M. Taut, J. Phys. C: Solid State Phys. **18**, 2691 (1985); K. Sturm, Phys. Rev. B **52**, 8028 (1995).

[28] V.L. Moruzzi, J.F. Janak, and A.R. Williams, *Calculated Electronic Properties of Metals* (Pergamon, New York, 1978).

[29] J.C. Boettger and S.B. Trickey, Phys. Rev. B **45**, 1363 (1992).

[30] K. Karlsson and F. Aryasetiawan, Phys. Rev. B **52**, 4823 (1995).

[31] C. Eppacher, R. Díez Muiño, D. Semrad and A. Arnau, Nucl. Instr. Meth. B **96**, 539 (1995).

[32] J.F. Janni, Atom. Data Nucl. Data Tabl. **27**, 147 (1982).

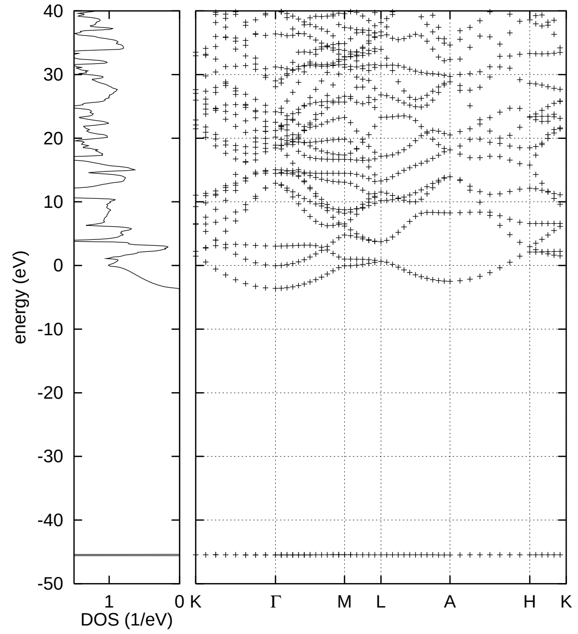


FIG. 1. Band structure of hcp lithium at lattice parameters $a = 5.65$ a.u. and $c = 9.26$ a.u. from GTOFF using the Moruzzi–Janak–Williams parametrization[28] of the Hedin–Lundqvist LDA to the exchange-correlation energy. The KS basis 41111/111/11, $5s3p2d$, is a partially de-contracted set of the "interior" layer set in Ref. 29, augmented by two $d$-type GTOs with exponents 0.36 and 0.14 taken from Ref. 7. $d$-type "polarization" functions are essential to avoid a spurious band-gap $\approx 20$ eV above $\varepsilon_F$.[30]

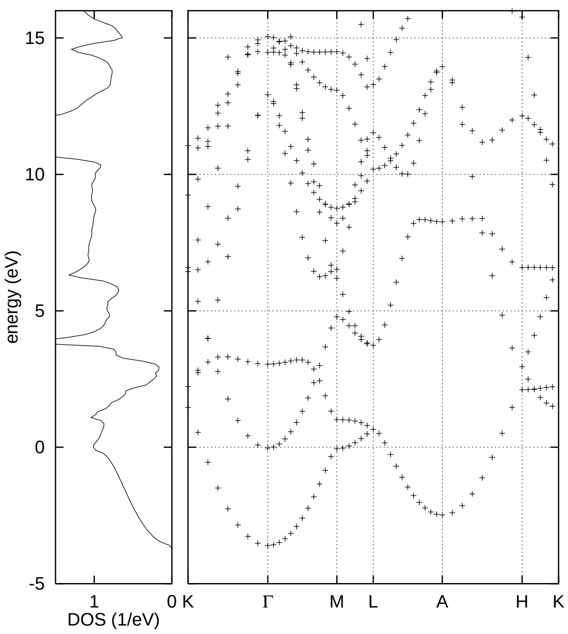


FIG. 2. Magnified view of Fig. 1. $\varepsilon_F$ is at 0 eV.

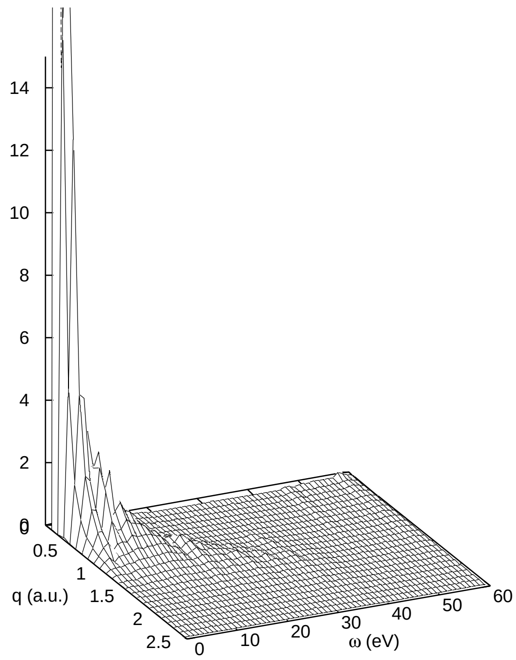


FIG. 3. Calculated $\Im\epsilon_{\mathbf{GG}'}$ of hcp Li for $\mathbf{G} = \mathbf{G}' = \mathbf{0}$. $\mathbf{q} \parallel (10\bar{1}0)$. Figs. 3–5 have been calculated starting from a DFT input with $12 \times 12 \times 6$ $\mathbf{k}$-points in the BZ (76 points in the IBZ).

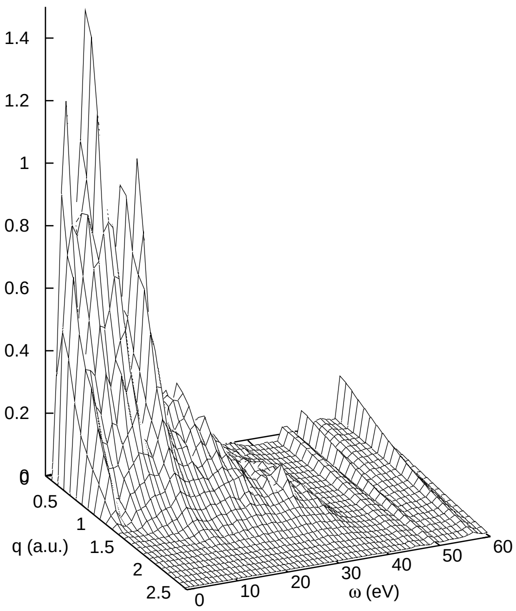


FIG. 4. $\Im\epsilon_{\mathbf{GG}'}$ for $\mathbf{G} = \mathbf{G}' = (0001)$. $\mathbf{q} \parallel (10\bar{1}0)$.

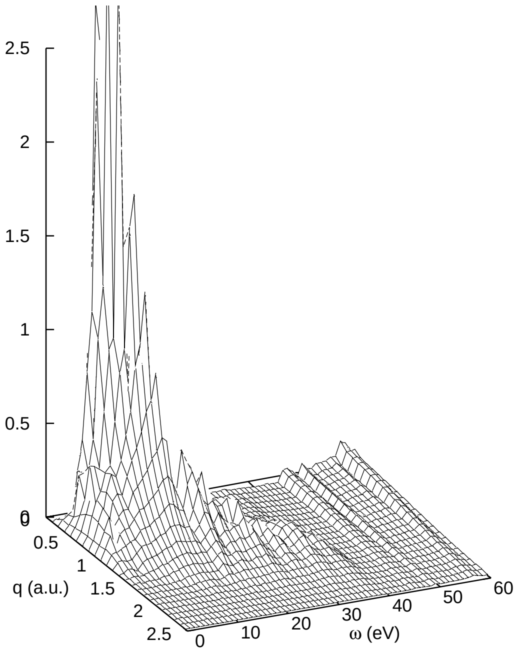


FIG. 5. $\Im[1/\epsilon_{\mathbf{0},\mathbf{0}}(\mathbf{q},\omega)]$. $\mathbf{q} \parallel (10\bar{1}0)$.

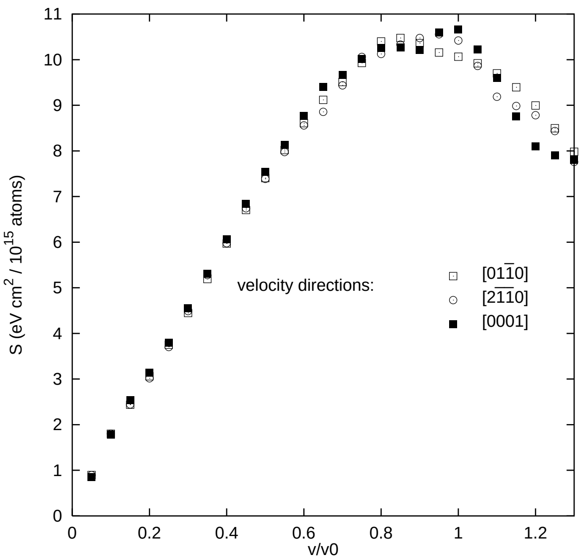


FIG. 6. Electronic stopping cross-section. $v_0$ is the Bohr velocity. The stopping power was integrated on a $23 \times 23 \times 29$ mesh in $\mathbf{q}$-space (parallelepiped $4.7 \times 4.7 \times 4.75$ a.u.$^3$) and on a mesh with 30 points in $\hbar\omega$-space (0...68.0 eV). The lowest twenty bands were included in the sum over band-pairs in (2). Augmentation of the $1 \times 1$ dielectric matrix to a $3 \times 3$ matrix by inclusion of the "indices" $\mathbf{G} = (0001)$ and $\mathbf{G} = (000\bar{1})$ does not lead to visible changes.

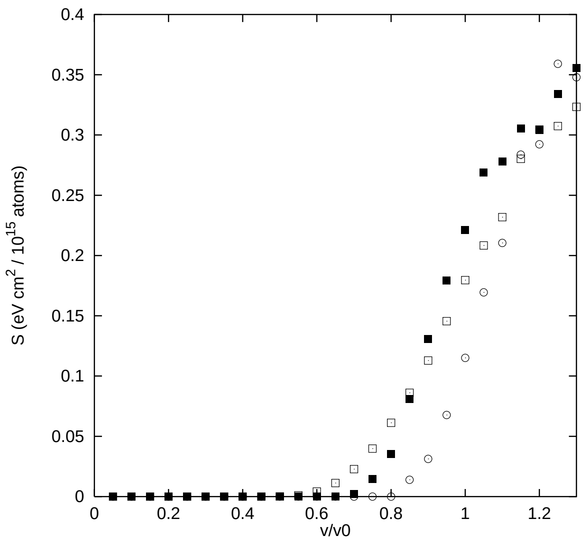


FIG. 7. If $\Pi$ is calculated without contributions from the valence bands, i.e. with $K$-shell excitations alone, but with other parameters kept as in Fig. 6, the cross section exhibits a non-linear behavior which reflects the effective band-gap of $\hbar\omega_g \approx 45$ eV for this case; recall Fig. 1. The threshold velocity of $0.8 v_0$ is approximately $\omega_g/k$, where $k$ is the wave vector on the free-electron energy shell, i.e., $\hbar^2 k^2/(2m) \equiv \hbar\omega_g$.

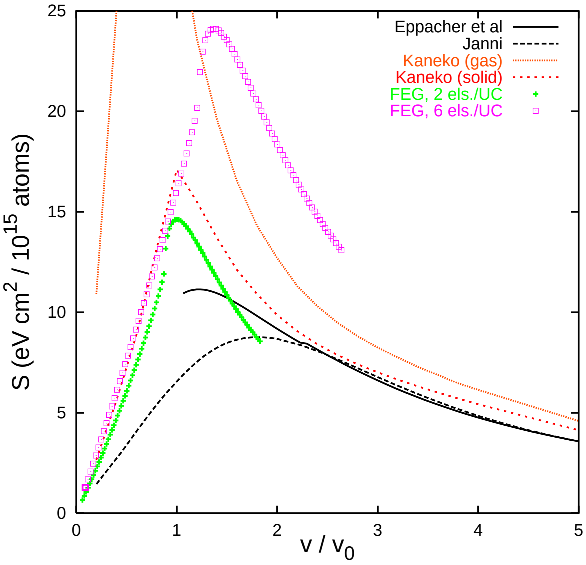


FIG. 8. Experimental proton stopping cross-section of (probably bcc) Li by Eppacher[31] and Janni,[32] compared with calculated values for gaseous and solid Li from the Kaneko[12] theory and RPA[10] free electron gas (FEG) values with a homogeneous density equivalent to 1 or 3 electrons per Li atom as shown.